Stochastic diffusion characterises early colony formation in Mediterranean coral Corallium rubrum

Ozan Kahramanoğulları, Bruna Giordano, Jonathan Perrin, Daniel Vielzeuf, Lorenzo Bramanti

Stochastic diffusion characterizes early colony formation in Mediterranean coral *Corallium rubrum*

Ozan Kahramanoğulları[a], Bruna Giordano[b,c], Jonathan Perrin[d], Daniel Vielzeuf[e], Lorenzo Bramanti[b]

[a] *Faculty of Computer Science, Free University of Bolzano-Bozen, Bolzano, Italy*
[b] *CNRS-Sorbonne Université, Laboratoire d'Ecogéochimie des Environnements Benthiques, LECOB, Observatoire Océanologique de Banyuls sur Mer, Banyuls sur Mer, France*
[c] *University of Cagliari, Department of Life and Environmental Sciences, Cagliari, Italy*
[d] *Synchrotron SOLEIL, L'Ormes des Merisiers, Gif sur Yvette, France*
[e] *Aix Marseille Université, CNRS UMR 7325, Centre Interdisciplinaire de NanoScience de Marseille, Marseille, France*

Abstract

The colony formation in Mediterranean coral *Corallium rubrum* is initiated by a larva that metamorphoses into the first polyp of the emerging colony approximately two weeks after settlement. The primary polyp then sets up a slow process that eventually, at least after several years, gives rise to a tree-like rigid colony structure on which other polyps flourish. For a mature colony, this axial skeleton provides support for new polyps. However, the first emergence of the characteristic axial skeleton takes two to four years from the larva stage. The early colony morphology, instead, is shaped exclusively by the polyps' abundant deposition of sclerites, a magnesian calcite biomineral that has a different granularity from the distinctive red-coloured skeleton. With the appearance of the first polyp, a growing sclerite heap in a mesoglea layer provides a base for the emerging colony. In this paper, to elucidate the mechanical processes of early skeleton development in *C. rubrum* colonies, we present a computational model whereby the mesoglea layer provides a diffusion medium for the sclerites that the polyps deposit. We show that our stochastic model with three parameters captures the dynamic variability observed in measurements on living colonies. Our simulation results provide evidence for a diffusion process whereby the

Email address: ozan.kah@gmail.com (Ozan Kahramanoğulları)

interplay between polyp budding and sclerite deposition are the main determinants of structure in early colony formation. Our model demonstrates that the frequency of budding events in an early colony can be described as a function of the available mesoglea surface whereas the number of polyps on the colony plays a secondary role in determining this frequency. We show that these model predictions are confirmed by direct observations on the colonies in our sample. Moreover, our results indicate that diffusion is a prevalent mechanism of colony development also at later stages of a colony's life span.

Keywords: Mediterranean coral, *Coralium rubrum*, early development, morphology, stochastic, diffusion

---

Introduction

Corallium rubrum is an octocoral, endemic to the Mediterranean and neighbouring Atlantic rocky shores at depths between 10 and 800 m and at temperatures up to 22 degrees Celsius [1, 2, 3, 4, 5, 6, 7, 8]. Due to the distinct red colour of its axial skeleton, the species is often referred to as the Mediterranean red coral (see Fig. 1A). Like other coral species, *C. rubrum* is an ecosystem engineer; their tree-shaped colonies contribute to the three-dimensional structuring of coralligenous assemblages, consequently providing shelter to other species and enhancing the associated biodiversity [9, 10, 11]. Thus, the well-being of *C. rubrum* colonies is a significant indicator of the state of their surrounding ecosystems. Its red calcareous skeleton has a high economic value as raw material for jewellery [12], hence extensive harvesting creates pressure on this species, thereby bringing it to the focus of conservation efforts [13, 10].

C. rubrum is a slow-growing species, and a colony's life span can exceed 100 years [1, 14, 8, 15, 16, 10]. As other colonial cnidarian, the species has a complex life cycle, involving sexual and asexual reproduction. Larvae, which start the colony, are the products of internal fertilisation [17]. When the colony is sexually mature, 6 to 10 years after settlement, it eventually produces larvae by sexual reproduction [18, 19]. The embryonic period lasts about a month

during summer [20]. Larvae originate from fertilised oocytes and exist only during this one-month period [21]. When a larva settles on a suitable substrate, it metamorphoses into the first polyp of the colony. All the other polyps of the colony, genetically identical to the first one, are produced asexually by budding, arising from the coenenchyme, the living tissue that covers the entire colony [1].

C. rubrum fecundity is reported to range between 1.0 ± 0.7 and 3.2 ± 2.3 mature gonads per polyp in female colonies and between 2.5 ± 1.6 and 6.9 ± 2.5 mature gonads per polyp in male colonies [22]. Sexually mature *C. rubrum* colonies release their larvae with a mean female polyp fecundity of 0.87 larvae per polyp [20]. *C. rubrum* larvae (planulae) are characterized by a high swimming activity, spending most of the time swimming up in the water column before metamorphosing in primary polyps [21]. The median survival time of the planulae in the water column has been measured as 32 days with a standard deviation of 11 days [23]. The larvae have a negative buoyancy with free-fall speeds between 0.03 and 0.09 $\mathrm{cm} \cdot s^{-1}$ and a mean upwards swimming frequency of 82 % [24]. The colony development starts with the metamorphose of the larva into a juvenile polyp within two weeks after its settlement on a suitable substrate [16].

The colony morphology of *C. rubrum* is characterised by a mostly inorganic rigid structure that is built by hundreds of polyps which are renewed several times along the colony's life span [25, 26] (see Fig. 1 A, B). The average age of colonies at first branching is 10 years with a standard deviation of 9 years; it can take a few decades until the colonies obtain a recognisable tree-like structure [14]. As the axial skeleton develops, it constitutes further support for the budding polyps, thereby facilitating the growth of the colony. The polyps, in return, contribute to the slow expansion of the tree-like structure, consequently facilitating the feeding of the emerging polyps by optimising their access to the surrounding environment [27].

The skeleton of *C. rubrum* is composed of two calcium carbonate ($CaCO_3$) structures, fabricated via distinct processes and tissues [1, 28] (see Fig. 2 A). The first one, the axial skeleton with the characteristic red colour, is com-

posed of magnesium-rich calcite with a small percentage of organic components [28, 29, 30, 31]. The second component corresponds to sclerites, which are grains of magnesian calcite, with a characteristic shape, embedded in the living tissues of the coral [32, 31]. The axial skeleton displays two distinct zones: a fast-growing medullary part surrounded by a slow-growing annular zone. Sclerites, cemented together, play a role in the construction of the medullary part (block-by-block growth mode), while the annular part is made of annual growth rings (layer-by-layer growth mode) [33, 34, 31]. The coenenchyme tissue that surrounds and links the polyps accommodates a mesoglea layer with sclerites that give a granular appearance to the living tissue. The sclerites initially form intracellularly in a primary scleroblast and continue to grow in an extracellular medium composed of two secondary scleroblasts. Mature sclerites then extrude into the mesoglea [28, 35]. The specific morphology of the sclerites differ between various corals and serves as a means for taxonomical identification [36, 37, 38]. With its hard calcitic skeleton obtained by $CaCO_3$ deposition, *C. rubrum* like other members of the family *Coralliidae* represent an exception in the order of *Alcyonacea*. The majority of these species have either a flexible axial skeleton formed by a horny complex protein (gorgonin) or a skeleton formed by sclerites which can be more or less aggregated depending on the species. *C. rubrum* skeleton uses magnesian calcite as a material, however with a distinctive specialisation that excludes a proteinaceous structure.

Although the red coloured axial skeleton is a recognisable feature of this species, its development requires the initial maturation of the colony, and it starts to form only when the colony reaches two to four years of age after the initial settlement of the larva [25, 33, 34, 31]. The initial colony structure is, instead, marked only by the sclerites [39]. Sclerite deposition starts approximately two weeks after the settlement of the larva and continues throughout the entire life of the polyps. As a result, the early colony development gives rise to a heap-like morphology that lacks an axial skeleton (see Fig. 1 C, D, E).

The functional role of sclerites, from an evolutionary point of view, has been hypothesised by various authors. Beyond their role in the axial skeleton makeup,

according to Allemand [40], one of the main functions of *C. rubrum* sclerites is to provide mechanical protection against abrasion. Lewis and Von Wallis [41] propose that sclerites may enable the bending capacities of some gorgonians. Kingsley [42] argues for the case of the gorgonian *Leptogorgia virgulata* that sclerites have multiple functions, including sensory and stability functions as well as protection against predators and abrasion.

In early colony development, sclerites are observed as the exclusive calcite building blocks [39]. Moreover, the growth mechanism of the early stage colonies and at the tip of the adult colonies share similarities [33]. In this paper, to elucidate the role of sclerites in colony development, we present a computational model of the processes that deliver the heap morphology, characteristic of the first years of ~~the~~ life of the colonies. Our model formally describes the physical environment of an initially seeded polyp, which is altered by three processes working in concert. These are: (*i*) the deposition of sclerites by polyps, (*ii*) the diffusion of the sclerites, and (*iii*) the budding of a new polyp. To accommodate the inherent stochasticity of these three processes and the small number of polyps, we have implemented a simulator that is based on Gillespie's stochastic simulation algorithm [43].

In the following, we show that our model, based on these three processes, captures the phenotypic variability observed on living colonies. Our model is based on a discretisation of space so that diffusion of sclerites on a grid representation can be accommodated and the dynamic evolution of the colony morphology in time can be monitored. This way, we could assess our model by comparing its morphological features with measurements on living colonies. Results indicate that the budding of new polyps in an emerging colony is a function of the available surface to the colony. Moreover, the number of polyps affects the expansion of the diffusion surface where the new budding events occur. Consequently, the number of polyps on the colony has an indirect effect on the budding events due to the surface that the emerging polyps expand. Inline with findings in previous studies [44], our results indicate that diffusion plays a prevalent role in colony development, not only in the first years of the

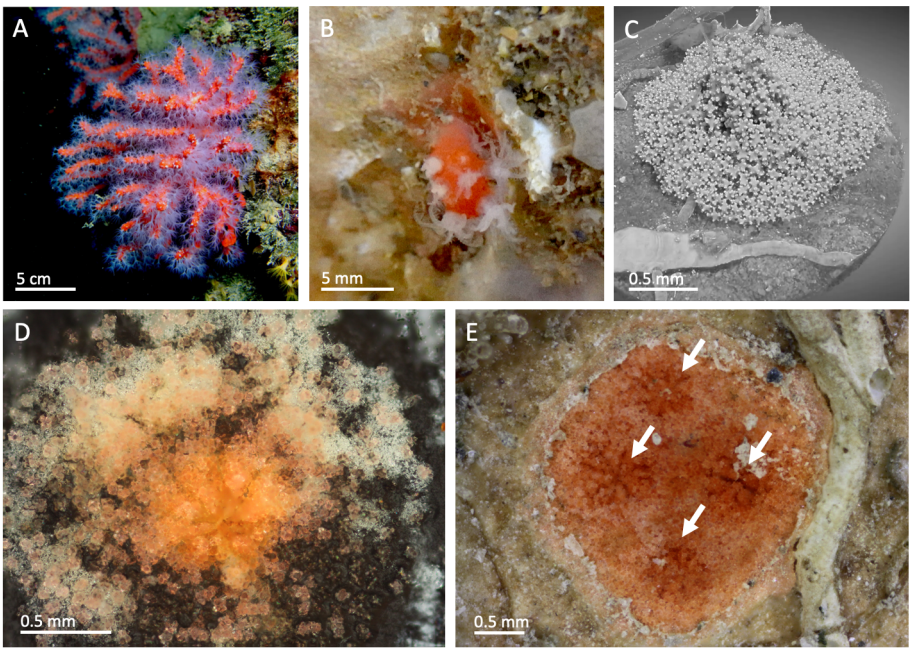

Figure 1: Images of *Corallium rubrum* colonies with various ages. (A) A mature colony. (B) A colony of 3 years of age. (C) SEM image of a 3 months old colony. (D, E) Light microscopy images of recruits that are 17 days old and 2 years old, respectively. The four polyps in (E) are indicated with arrows.

emerging colony, but also in mature colonies. Overall, our results demonstrate how field and laboratory data can be integrated within numerical models for a quantitative understanding of the growth processes. Due to the long life span of the corals and their developmental processes, models provide invaluable instruments to understand processes that are hard or costly to observe in real-time.

Materials and methods

Data acquisition

The *C. rubrum* colonies used for the measurements were obtained from larvae settled and developed in a system of artificial caves, located at 30 m depth near the southern border of the Marine Reserve Cerbere/Banyuls (North-Western

Mediterranean Sea, France). In 2018, adult male and female colonies were implanted upside down on terracotta tiles (20 × 20 cm) placed on the vault of the artificial caves, just before the larval release of *C. rubrum* in late July [20]. The artificial cave system is conceived to accommodate the collection of the terracotta tiles and their transport to the laboratory aquarium. In June 2019, 120 recruits, result of the 2018 larval settlement, were found on the tiles. These tiles were collected and brought to laboratory to perform an accurate measurement of the diameter of the settled colonies. After the measurements, the tiles were placed back in the artificial caves system. The same operation was repeated in June 2020 to measure the diameter of the 2 years old colonies (Fig. 2 C, D). The final dataset of 61 colonies consists of those colonies on which diameter was measured in 2019 and that were still alive in 2020. The measurements were performed on the photos taken using a high-resolution camera mounted on a stereomicroscope (Zeiss Scope) and calibrated with micrometer slide (precision 0.01 mm).

In parallel with the procedure above, to determine the timing of sclerite production we used larvae settled in aquarium tanks. To obtain settlement in aquarium, sexually mature *C. rubrum* colonies were collected in late July 2018 and 2019 before larval release [20] between 25 and 35 m depth. The colonies were collected in the area adjacent to the Marine Reserve Cerbere/Banyuls. After collection, the colonies were transferred to open circuit aquaria with air bubbling and maintained at 16–18° C. To ensure oocyte fertilisation, the corals were re-arranged to contain females and males in the same closed-circuit aquaria. The aquaria were surveyed daily for larval release, which began on August 5th, 2018, and July 22nd, 2019, and concluded within 10 days. The larvae were transferred to closed circuit, oxygenated and temperature-controlled aquaria, and offered suitable settlement substrates [21]. All the aquaria were subjected to two LED white lights under a cycle of 12-h light and 12-h dark (see [21] for details). After larval settlement and the metamorphosis into polyps, all the colonised substrates were re-transferred to open circuit aquaria with an air bubbling system and observed and photographed with a dissection microscope

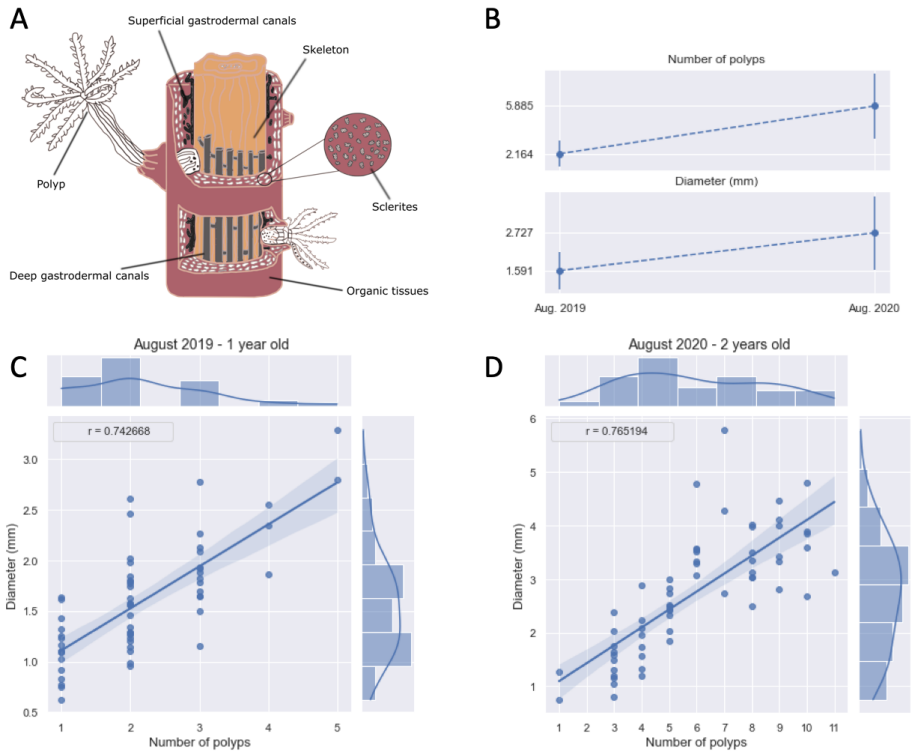

Figure 2: (A)Diagrammatic representation of two distinct calcification processes in *C. rubrum* polyps. (B, C, D) Measurements on 61 colonies as described in the materials and methods section. Mean and standard deviation of number of polyps and diameter after a year and after two years after initial settlement (B). Number of polyps and colony diameter correlation in colonies after one year (C) and after two years (D); r is the Pearson correlation coefficient.

every day to check for the presence of sclerites.

The basal diameter of each colony was obtained by averaging two measurements corresponding to (*i.*) the maximal spatial extent of the colony along any orientation in a plane parallel to the settled surface, and (*ii.*) the corresponding maximal spatial extent along an axis perpendicular to the first [7, 14].

The statistical features of the sample data are depicted in Fig. 2. The mean and the standard deviation of the number of polyps and the diameter after a year and after two years after initial settlement are depicted in Fig. 2 B. The figure includes the Pearson coefficient quantifying the correlation between the

number of polyps and colony diameter in colonies after one year (Fig. 2 C) and after two years (Fig. 2 D).

Stochastic diffusion model

The base of the emerging colony is discretised with a two-dimensional grid representation whereby the sclerites are allowed to stochastically diffuse between cells [67]. The mass of each sclerite is $0.16 \pm 0.08\,\mu g$ and the $CaCO_3$ deposition rate is measured as $4.34 \pm 2.23\,\mu g$ (SD) per day [45]. The choice of the grid resolution affects the simulation efficiency such that a higher resolution model results in slower simulations. To increase the simulation efficiency, the size of each deposition unit was set proportional to the daily deposition mass of *C. rubrum* polyps. Consequently, each cell corresponds to approximately 27 sclerites of cubic volume, where each basal side of the cube has a length of 3 sclerites, each with an approximate size of 60-100 μm and a characteristic dumbbell shape [1, 46, 47]. Thus, in our simulations, each $\mathsf{Sclerite}$ entity corresponds to a deposition unit of sclerites with a mass of $4.34 \pm 2.23\,\mu g$.

We formalised the events of the system as a chemical reaction network (CRN), which implements mass action dynamics. We then mapped the model representation to a grid structure for efficient processing as described below. In the CRN representation, a reaction of the form $\ell \xrightarrow{\tau} \rho$ consumes the entities ℓ from the state and produces the entities ρ with a stochastic rate τ. The time unit of each event is in *weeks*.

The reactions modify the cells of the grid. Each cell can accommodate a maximum of one polyp. The initial state with the primary polyp at the centre of the grid is given by $\mathsf{Polyp}_{0,0}$ and we have $\mathsf{Empty}_{i,j}$ for all (i, j) pairs except $(0, 0)$, which indicates that there is no polyp at these cells. If a polyp is present in a cell, it can deposit a unit of sclerites with a rate of r_{dep}. The *deposition* rate of sclerites is bounded by the metabolic processes of each polyp [48]. Consequently, it is described in our model by stoichiometry with a stochastic rate that captures the variability. Thus, for a polyp in a cell with the indexes i and j, the deposition

is given by a first-order reaction

$$\mathsf{Polyp}_{i,j} \xrightarrow{r_{dep}} \mathsf{Polyp}_{i,j} + \mathsf{Sclerite}_{i,j}$$

where i and j are the coordinates of that cell on the grid. Each cell can have arbitrarily many sclerite units stacked on each other and the number of Sclerite units in the stack correlates with the height of the colony at that location.

For the *diffusion* with rate r_{dif} of a Sclerite at a cell with the index i, j, we have the following first order reactions.

$$\mathsf{Sclerite}_{i,j} \xrightarrow{r_{dif}} \mathsf{Sclerite}_{i+1,j} \quad \mathsf{Sclerite}_{i,j} \xrightarrow{r_{dif}} \mathsf{Sclerite}_{i-1,j}$$
$$\mathsf{Sclerite}_{i,j} \xrightarrow{r_{dif}} \mathsf{Sclerite}_{i,j+1} \quad \mathsf{Sclerite}_{i,j} \xrightarrow{r_{dif}} \mathsf{Sclerite}_{i,j-1}$$

Due to the mass action dynamics, sclerites diffuse from higher cells to the lower.

For the budding events, we work with a reaction scheme of the form

$$\mathsf{Empty}_{p,q} + \mathsf{Sclerite}_{p,q} + \mathsf{Polyp}_{i,j} \xrightarrow{r_{bud}} \mathsf{Sclerite}_{p,q} + \mathsf{Polyp}_{i,j} + \mathsf{Polyp}_{p,q}$$

where r_{bud} is the budding rate, $i \neq p$, $j \neq q$ and there exists at least one sclerite at the cell p, q, which also indicates that the cell is reachable by diffusion. The presence of a sclerite models the presence of the living coenenchyme tissue with a mesoglea layer where the new polyps can stochastically bud. The polyps do not diffuse; once they stochastically bud, they stay fixed at that position.

In the simulations, we resort to the notion of *propensity* as defined in the stochastic simulation literature, see, e.g., [43, 49, 50]. To assess the applicability of different models as a function of the number of polyps in the colony, the budding propensity a_{bud} is computed with the following expression:

$$a_{bud} = \frac{\#\mathsf{Polyp} \cdot r_{bud}}{\#\mathsf{Polyp}^{\mathsf{be}}} \tag{1}$$

The case with the *budding exponent* $\mathsf{be} = 0$ corresponds to a standard first-order semantics of this reaction (because the numbers of $\mathsf{Polyp}_{i,j}$ and $\mathsf{Empty}_{i,j}$ can both have a maximum value of 1 at any state). On the other hand, a value of $\mathsf{be} = 1$ delivers a zero-order-reaction semantics, whereby budding propensity

is independent of the number of polyps. The values of $0 < \mathsf{be} < 1$ deliver the intermediate cases.

$$\mathsf{be} = 0 \;\Rightarrow\; a_{bud} = \#\mathsf{Polyp} \cdot r_{bud} \qquad \text{and} \qquad \mathsf{be} = 1 \;\Rightarrow\; a_{bud} = r_{bud} \tag{2}$$

Because polyps have an average life span of 12 years [26], in our model that covers the first two years of the colony, polyp death is negligible, hence not included.

We implemented the simulations in OCaml according to the Gillespie [43] algorithm. Our algorithm accommodates a matrix data structure for representing the grid for better performance in comparison to a standard CRN representation. Consequently, the model state is given by a matrix of pairs (m, n), where m is the number of Sclerite units in that cell and n is a boolean variable indicating if there is a polyp in that cell. As described above, each simulation step updates the grid according to the CRN reaction. For example, an instance of the deposition reaction at the cell i, j updates that cell $(m, \texttt{true})$ as $(m+1, \texttt{true})$. In our implementation, diffusion at the boundaries have no effect. However, we implemented a grid size with 101 $\times$ 101 cells, which rendered the boundary conditions redundant. In comparison to the standard algorithm, our implementation updates the propensities only for the affected reactions after each simulation step as in the Gibson-Bruck algorithm [51] with performance improvement. We performed the simulations on a 30 node HPC server and obtained the measurements as the mean of the repeated simulations together with their SD values.

The range of model parameters was narrowed down and the parameters are fitted by considering the mean number of polyps in the sample at the end of the first year and the second year (Fig. 2). For the daily sclerite deposition rate, we used $4.34 \pm 2.23g$ (SD) per day as a baseline [45]. Because each Sclerite unit models this mass, we explored the simulation dynamics in the neighbourhood of $r_{dep} = 7\ week^{-1}$ to fit the parameters r_{dif}, r_{bud}, and be. The number of repeated stochastic simulations for each parameter set is chosen to provide a sufficient number of data points with a clear trend along neighbouring parameter regimes.

We have first performed sweeps of simulations to obtain parameter combinations that deliver a mean of 2.2 polyps at the end of the first year and 5.9 polyps at the end of the second year according to the values found in our samples. To further narrow down the parameter space, we have implemented a gradient descent algorithm based on the mean polyp counts of each simulation batch and factors for the stochasticity according to the sample SD.

For the model visualisations, we mapped the simulation data to a 3D graphical representation based on the positions of the entities on the grid structure via a Javascript implementation that uses the *Three.js* library. For the 3D-modelling of the sclerite object we used the Vectary software.

Results

Fig. 3 shows the trends of the relationships between model parameters that are fit to the sample data of polyp counts. Each point on a curve indicates a set of values for the parameters r_{dep}, r_{dif}, and r_{bud} for $\mathsf{be} \in \{0, 0.5, 1\}$ that are colour coded. The fully coloured curves indicate the fit r_{bud} rate at the end of the second year, whereas the dashed curves indicate a fit at the end of the first year. Consequently, the sets of parameters that produce a model behaviour consistent with the sample data are given by those points in the regions in Fig. 3. The parameter regimes where the dashed and fully coloured curves intersect are those that provide a perfect fit to the mean of the sample data. Accordingly, the parameter regimes with a fit to the sample, including a margin of error, are characterised by $\mathsf{be} = 1$ values, however with lower diffusion rates above 0.01 (Fig. 3 B). On the other hand, for $\mathsf{be} = 0$ and $\mathsf{be} = 0.5$, a fit is obtained at higher diffusion rates. In addition, in all regimes, the r_{bud} rate values inversely correlate with the r_{dep} rate.

We have verified the fit parameter spectrum in several steps. We have first compared the simulated standard deviation in the measurements of the number of polyps with those of the sample (Fig. 4). We have analysed the SD of the number of polyps in the colony in relation to the effect of the parameter be on

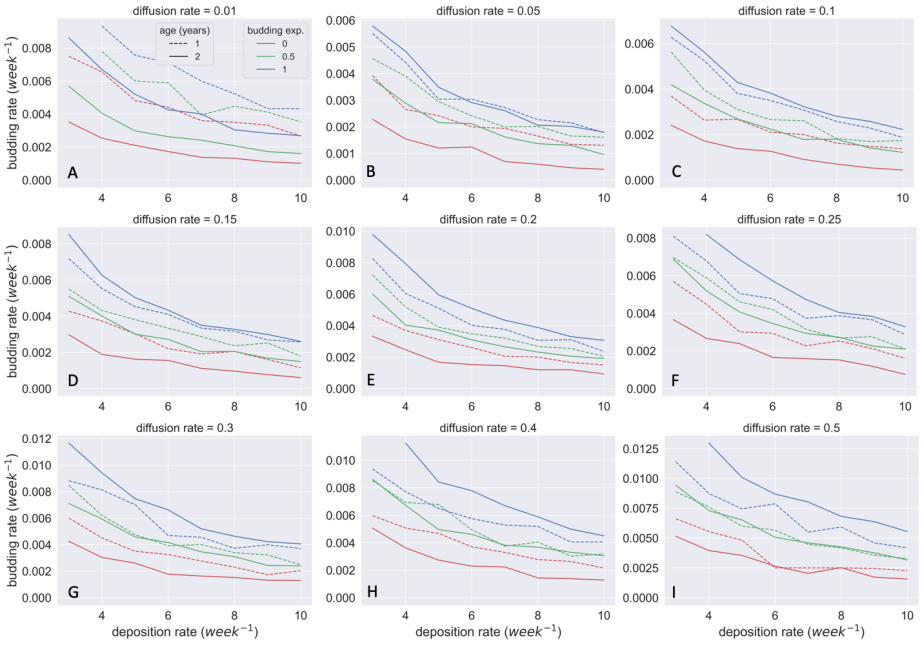

Figure 3: Fit parameter sets for different budding exponent be values and the rates r_{bud}, r_{dif}, and r_{dep}. As indicated in the legend, the fully coloured curves indicates a fit to the sample mean of 5.9 polyps per colony at the end of the second year. The dashed curves indicate a fit to the sample mean of 2.2 polyps per colony at the end of the first year. Diffusion rates are indicated at the top of each subplot.

the stochastic budding propensity of new polyps (see 1 and 2): for $\mathsf{be} = 0$, the budding propensity is directly proportional to the number of polyps in the colony, whereas, for $\mathsf{be} = 1$, this value is constant (see 1 and 2). Consequently, a be value of 0.5 indicates an intermediate setting in which the budding propensity is partially affected by the number of polyps in the colony.

As depicted in Fig. 4, for all the values of the diffusion rate r_{dif}, all the sets of parameters with $\mathsf{be} = 0$ result in a spread of the simulation distribution with SD values that are much greater than those observed in the sample data (Fig. 2). In particular, with a decrease in be, we observe that the SD values that are clearly distinct at the end of the first year are coupled with SD values at the end of the second year that have a proportionally increased amplification. In contrast, $\mathsf{be} = 1$ result in SD values that are in agreement with the sample data. Finally, with $\mathsf{be} = 0.5$, SD values are intermediate between those for $\mathsf{be} = 0$ and $\mathsf{be} = 1$. These observations suggest that the budding events depend only indirectly on the number of polyps in the colony. This partial dependence is present because the availability of a surface is a requirement for the budding of new polyps and sclerite deposition propensity, thus the spread of the mesoglea surface, is a function of the number of polyps in the colony. However, as defined in Equation 1, a propensity function that depends on the number of polyps in the colony with $\mathsf{be} < 1$ results in SD values that diverge from those observed on the sample data. This implies that the frequency of budding events are determined by the polyps in the colony only to the extent that they provide a budding surface. Consequently, the budding propensity remains constant as long as there is sufficient space for new polyps.

In the light of the results above, we used the $\mathsf{be} = 1$ as a baseline to evaluate the relationship between model parameters and the colony diameter in different parameter regimes. We observed that colony diameter correlates with the diffusion rate r_{dif}, colour-coded in Fig. 5 A, and it is only moderately affected by the deposition rate r_{dep} (Fig. 5 A). We then computed the correlation between the number of polyps and the colony diameter for each parameter set. In the next step, we compared these measurements with those with the sample. For

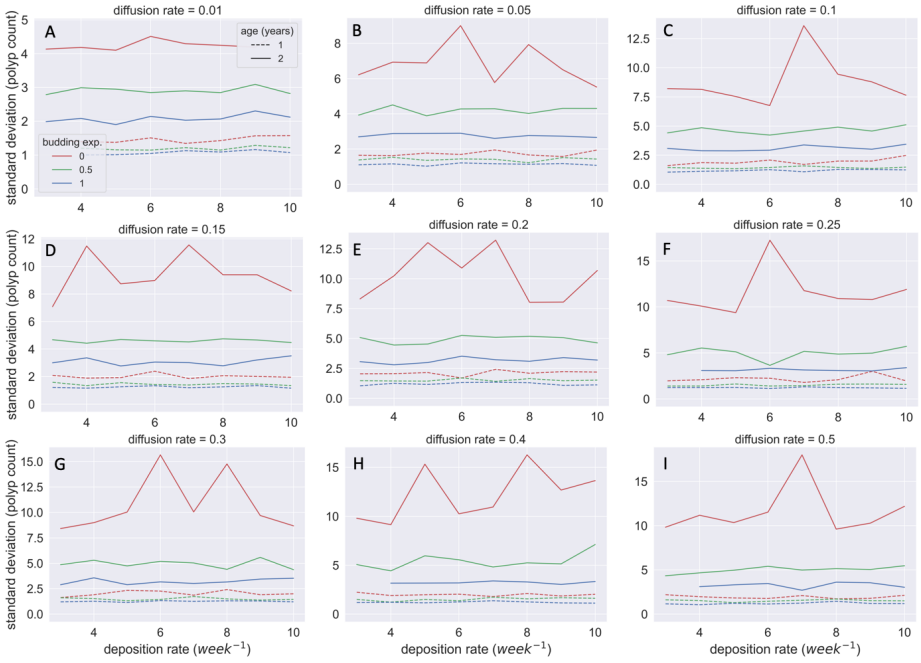

Figure 4: SD in polyp counts for the simulation batches in Figure 3. The colour codes correspond to different be values. As indicated in the legend, the full curves indicates a fit to the sample mean of 5.9 polyps per colony at the end of the second year. The dashed curves indicate a fit to the sample mean of 2.2 polyps per colony at the end of the first year. Diffusion rates are indicated at the top of each subplot. Budding rates r_{bud} are as those that correspond to the respective points on the curves for different be values in Figure 3.

this, we measured the correlation between the number of polyps in the colony and the colony diameter in terms of the Pearson correlation coefficient r and visualised it as a function of the model parameters (Fig. 5 B). We observed a correlation coefficient in agreement with the sample data (r Pearson > 0.6) for the parameter regimes in the interval given with ($r_{dif} = 0.15$, $r_{bud} = 3$) and ($r_{dif} = 0.3$, $r_{bud} = 10$).

In the following step, to evaluate the simulation results from a different point of view, we computed the ratio of the colony height to the colony diameter in the simulations. Because we do not have accurate measurements of colony height, we applied conservative thresholds to rule out the height to diameter ratios ≥ 1 as well as those ≤ 0.15. The rationale for the lower-bound is based on the known size of the sclerites (approximately 60–100 μm along the longer axis) and observations on images with a scanning electron microscope (SEM) as well as our knowledge of the species. Firstly, it is worth noticing that *C. rubrum* is an erect species, which tends to grow in height. A lower height to diameter ratio could have been possible for encrusting species (such as those belonging to the order Stolonifera). However, it is unrealistic for an erect species. From a quantitative point of view, we estimated the number of sclerite layers forming 3-months-old recruits (e.g. Fig. 1C). Even if the field of view of SEM does not permit a precise quantification of the layers, it is easy to estimate that the 3-month-old recruits are formed by at least 10 sclerite layers. The video in the S.I. shows the SEM image of this 3-months-old-recruit from various angles. With a conservative estimation of the heap height in correlation with sclerite size and the mean diameters of 1.59 mm and 2.7 mm measured on the 1-year old and 2-years old samples, we obtain height to diameter ratios that exceed 0.15. This sorting allowed us to exclude the implausible simulated morphologies that are either extremely spread or extremely concentrated. Filtering with such a consideration highlights again the parameter regimes within the interval given with ($r_{dif} = 0.15$, $r_{bud} = 3$) and ($r_{dif} = 0.3$, $r_{bud} = 10$), in agreement with the correlation between the number of polyps and the colony diameter (Fig. 6 B).

Finally, we have plotted the emerging colony morphologies by 3D anima-

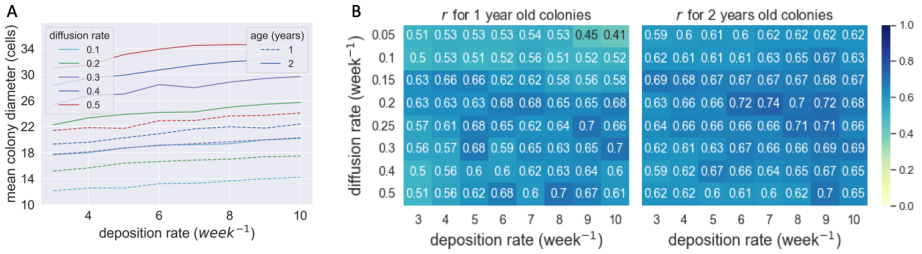

Figure 5: The relationship between model parameters and the colony diameter. (A) The colony diameter as a function of r_{dep} and r_{dif}. As indicated in the legend, the full curves correspond to two-years-old colonies and the dashed curves to one-year-old. (B) The correlation between the number of polyps in the colony and the colony diameter, measured in terms of Pearson correlation coefficient r after one year and after two years. Budding rates r_{bud} are those that correspond to the points on the be = 1 curve in Fig.3.

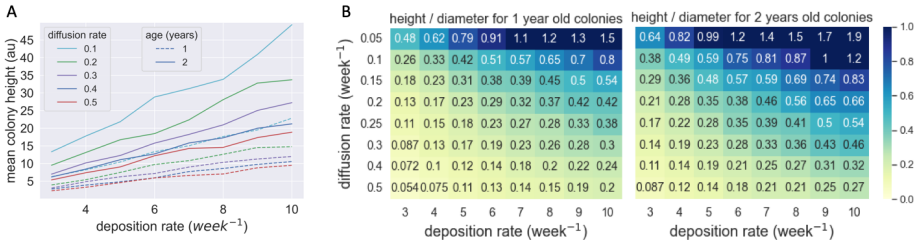

Figure 6: (A) The relationship between model parameters and the colony height. As indicated in the legend, the full curves correspond to two-years-old colonies and the dashed curves to one-year-old. (B) The height to diameter ratio of the simulated colonies after one year and after two years. Budding rates r_{bud} are those that correspond to the points on the be = 1 curve in Figure 3.

tions for visual comparison with sample images. The visual representations of the simulations show how shifts in sets of parameters result in different colony morphologies at the end of the first year (Fig. 7) and the second year (Fig. 8).

Discussion

The present work elucidates the mechanisms of growth in the early stages of the Mediterranean red coral *Corallium rubrum* development. *C. rubrum* growth is a slow process [14, 31] involving complicated interactions between

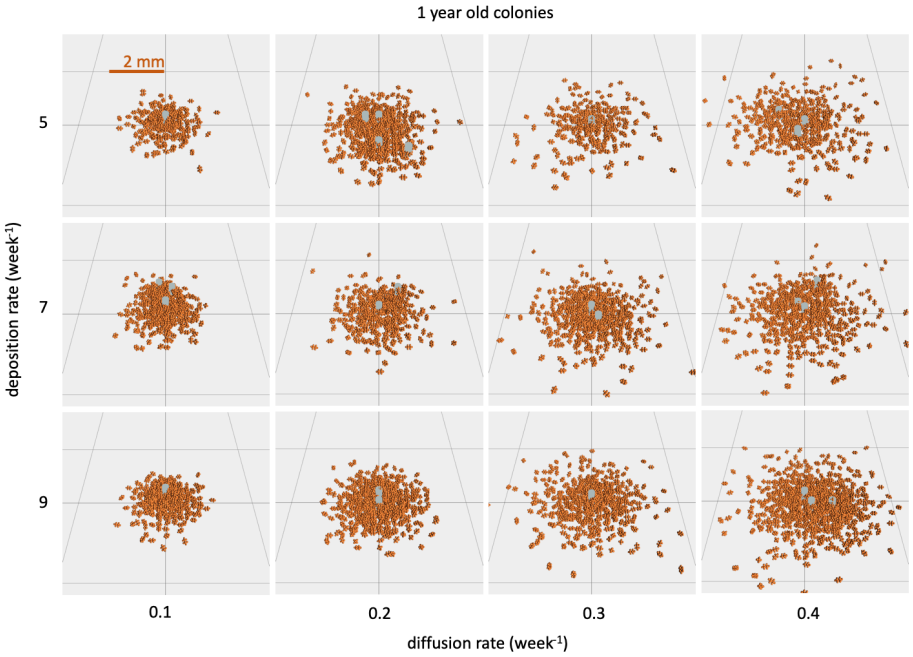

Figure 7: Representative graphical visualisations of simulated colonies after one year where the grey objects are the polyps. The emerging morphologies for these samples after two years are depicted in Figure 8.

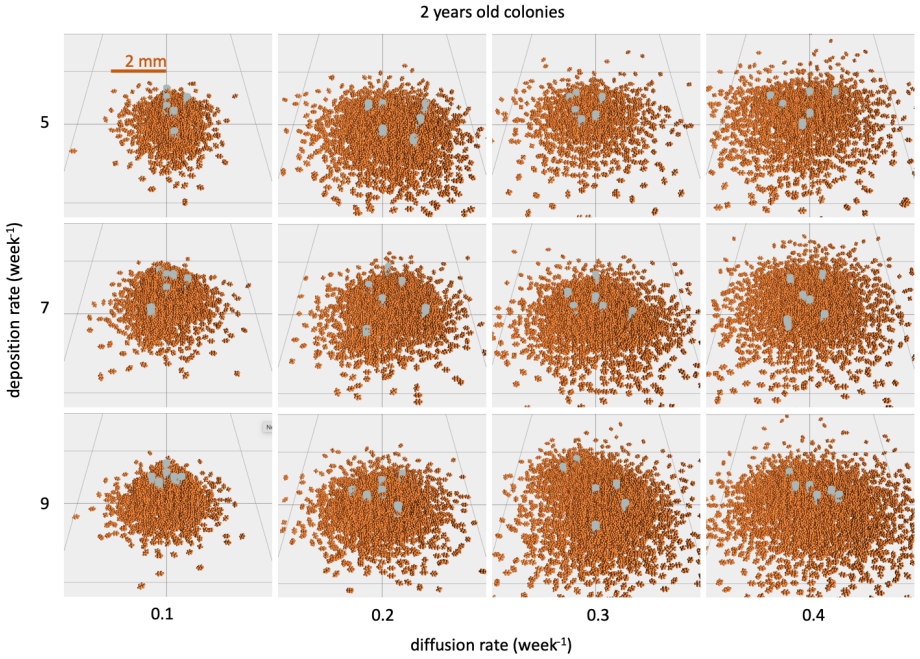

Figure 8: Representative graphical visualisations of simulated colonies after two years where the grey objects are the polyps The emerging morphologies for these samples after one year are depicted in Figure 7.

physical and biological processes, i.e., biomineralization. Two orthogonal approaches are commonly used to understand such processes: one is to observe each element of the phenomenon in detail by analytically breaking down the components. Another approach is abstracting away from details to focus on the principle components of the phenomenon.[1] In this respect, mathematical and computational models serve as instruments for formally describing the processes under examination. In such a setting, feedback from real-world measurements is crucial for assessing the model assumptions. This way, models can be refined and verified to converge at an improved understanding of basic mechanisms.

Mathematical and computational models of corals have been extensively studied from different points of view, e.g., [53, 54, 55, 56]. In [57], Kaandorp and Kübler bring together a volume that provides a comprehensive overview of the use of simulation models in studying various aspects of coral morphologies.[2]. Some of the works that built on the considerations in [57] are the following. In [60], Kaandorp and Sloot introduce two different simulation models and compare them to assess the effect on coral morphology of the local availability of food particles versus food particle distributions caused by a combination of flow and diffusion. In [61], Merks et al. refine the models in [60] with conclusions on morphological ranges in simulations and, in [62], Merks et al. present an alternative mechanism of branching for the model in [61], based on "polyp fanning effect" whereby polyps on a convex surface have a competitive advantage relative to polyps on a flat or concave surface. In [63], Kaandorp et al. use simulations to generate *Madracis mirabilis* morphologies that are virtually indistinguishable from the 3D images of the actual colonies. In [64], Laforsch et al. introduce a method to calculate the surface area in living scleractinian corals by using a combination of X-ray computed tomography and 3D modelling. In [65], Chindapol et al. refine previous considerations in a parameter-rich simula-

[1] See [52] for an excellent take on the role of modelling in describing natural phenomena.

[2] The book is a part of a series that includes similar considerations on sea shells [58] and plants [59].

tion model of growth and form properties of the scleractinian coral *Pocillopora verrucosa* and analyse how the coral morphology is influenced by the effect of water motion. In [66], Hennige et al. use a model comprised of two rules to characterise the conditions in which *L. pertusa* colonies effectively optimise their local flow requirements through habitat engineering.

Our model integrates information from analytical studies on *C. rubrum* development to isolate the processes driving the growth of newly settled individuals [25, 30, 33, 34, 31]. We have shown in [39] that the skeleton formation during the first 2 years of life in *C. rubrum* happens exclusively by sclerite deposition. Moreover, it is known that sclerite deposition happens at the base of each polyp. Still, how sclerite deposition is related to the number of polyps and other system components had remained unclear. Following observations on living samples, we hypothesised that the force driving the growth of the recently settled individuals is the diffusion of the sclerites through the acellular matrix given by the mesoglea layer. An alternative mechanism to diffusion is that the sclerite heap 'rises' similar to the growth patterns observed due to the deposition of calcium carbonate layers in the later stages of the colony's life. Sclerites and the red-coloured CO_3 of the axial skeleton are fabricated via distinct processes and tissues. The sclerites have a discrete makeup within the viscous mesoglea layer. In the light of this observation, we identified diffusion as the most prevalent potential mechanism that drives the early morphology in our samples. To test our hypothesis, the model was constructed around diffusion processes (see the material and methods section). To factor for the uncertainty in the position and the noisy frequency of budding events as well as their small number of occurrences in comparison to other processes, we resorted to a stochastic model.

We chose the diffusion model based on the law of mass action due to its simplicity. We have excluded more complex mechanisms because sclerite aggregates maintain a simple heap morphology deprived of any obvious patterns. Any other structures that are not reminiscent of a heap structure appear to form due to an alternative form on the medium that drives such a morphology. Gillespie's stochastic simulation algorithm [43, 51] provides an exact means for simulating

mass action kinetics in a stochastic setting. We used a standard compartment-based space discretisation to encode mass action [67]. Such models characterise the variability in the simulation trajectory due to discrete quantities, that is, sclerites and polyps, and small numbers of model species, that is, polyps.

We obtained the parameter range of our model by taking the daily sclerite deposition rate of polyps as a baseline [45] and fitting the mean and the standard deviation of the simulations results on the number of polyps to the measurements on our sample. With this baseline, given that the width of a unit on the model grid is in the order of 0.1 mm, the diffusion rate range of 0.1 to 0.5 units per week is in agreement with the expectations based on observations on living colonies. Within the range of parameters identified by our model, stochasticity in the simulations can explain some of the environmental factors that affect the colony. Moreover, the variations in emerging structures in simulations due to the changes in model parameters are also representative of the differences in environmental factors that affect the colony development. For example, the environmental conditions that provide increased access to nutrients, such as currents, could result in a slight increase in the deposition rate. Singling out these influences requires accurate data from controlled experiments, which can then be used to feed models. We consider the related research questions as well as those on the range of parameters in relation to plausible morphologies worthy of future investigation. In this regard, our model can be further developed to serve as a tool for understanding the impact of environmental factors in restoration programs. This way, researchers should be able to develop protocols to enhance larval settlement, thereby being able to forecast the growth dynamics in the very first stages of the coral life cycle, during which the colonies are not protected by a rigid axial skeleton.

Our model elucidates the budding of new polyps via diffusion only to the extent that the sclerite heap provides a surface on which new polyps can stochastically bud. The exact mechanism with which new polyps emerge remains as another topic of investigation for future work.

The dataset that we used to fit and verify the model is based on a two-

year study during which the diameter and the number of polyps of recently settled individuals were measured. Our simulations accurately reproduce the growth patterns of the young coral colonies, both quantitatively, i.e., the correlation between the number of polyps and the diameter, and qualitatively from a morphological point of view, i.e., Fig. 7 and 8. Our results, based on the combination of in situ and in silico experiments, allow us to confirm the hypothesis that *C. rubrum* growth within the first two years is fundamentally driven by processes linked to the passive diffusion of sclerites in the acellular matrix.

It has been observed on samples of seafloor litter, including a (plastic polyethylene) bag fragment, a plastic (polyvinyl chloride) tape fragment, and two ropes (polypropylene), as well as in experiments in controlled environments that the hydrophobic surface of plastic substrates provide a favourable medium for red coral settlement [44]. The colonisation pattern on these substrates follow the structure and shape of the plastic items and remains limited to these areas. The living coenenchyme tissue in *C.rubrum* covers the axial skeleton, thereby forming a layer on the external surface [1, 29]. In the light of these observations, given that sclerite deposition continues throughout the life span of the polyps and sclerites are incorporated at the tip of the branches [29, 33], the passive diffusion processes that are described by our model should be the prevalent mechanism in the colony development, not only in the first years after settlement but also later in the colony life.

Our analysis provides an overview of how stochastic simulation models can provide insights into the structure and development of modular organisms in a way that captures the inherent phenotypic variability. A similar approach should provide new insights also on later stages of the coral life cycle and the growth dynamics of adult colonies. Preliminary results in [27] indicate that a stochastic model accurately captures the morphological variability observed on living *C. rubrum* colonies. In this respect, in silico modelling of corals exposes new tools for marine biology and conservation ecology. This is partly because large-scale experiments on ecosystems are impractical or unethical at ecologically appropriate scales, and the demographic data on pristine populations are

often lacking. Formal models are powerful instruments, especially for studying coral species whose slow growth dynamics does not allow direct observation and experimentation. Stochastic simulations can remedy the lack of large scale or long term experiments, thereby elucidating the mechanisms at various levels in a way that would complement, guide and accelerate the fieldwork.

Supporting information

S1 File. **Sample data.** The sample data with the number of polyps and the colony diameter at the end of the first year and the second year.

S2 File. **Simulator source code.** The repository that contains the model source and the simulation algorithm written in OCaml https://github.com/ozan-k/ScleriteSimulation.

S3 File. A video that shows the scanning electron microscope (SEM) image of the 3-months-old-recruit in Fig. 1C from various angles.

Acknowledgments

The research leading to these results received funding from the European Union's Horizon 2020 research and innovation programme under grant agreement No 730984, ASSEMBLE Plus project UNICOMS, "Understanding Coral Colony Morphology via Stochastic Modelling", and from Prince Albert II of Monaco Foundation. This research was partially conducted during O.K.'s appointment at the University of Trento, Department of Mathematics. The authors thank Noemi Toni for preparing Fig. 2 A.

References

References

[1] H. Lacaze-Duthiers, Histoire naturelle du corail, J. B. Bailiére et Fil, Paris, 1864.

[2] H. Zibrowius, M. Montero, M. Grashoff, La re-partition du *Corallium rubrum* dans l'Atlantique, Thetys 11 (1984) 163–170.

[3] H. Chintiroglou, C. Dounas, A. Koukouras, The presence of *Corallium rubrum* (Linnaeus, 1758) in the Eastern Mediterranean sea, Mitteilungen aus dem Zoologischen Museum in Berlin 65 (1989) 145–149.

[4] R. Cattaneo-Vietti, F. Cicogna (Eds.), Il corallo rosso in Mediterraneo: Arte, Storia e Scienza, Red Coral in the Mediterranean Sea: Art, History and Science, Ministero delle Politiche Agricole, Alimentari e Forestali, Rome, 1993.

[5] S. Rossi, G. Tsounis, C. Orejas, T. Padron, J. Gili, L. Bramanti, N. Teixido, J. Gutt, Survey of deep-dwelling red coral (*Corallium rubrum*) populations at Cap de Creus (NW Mediterranean), Marine Biology 154 (2008) 533–545.

[6] F. Costantini, M. Taviani, A. Remia, E. Pintus, P. J. Schembri, M. Abbiati, Deep-water *Corallium rubrum* (L., 1758) from the Mediterranean Sea: preliminary genetic characterisation, Marine Ecology 31 (2010) 261–269.

[7] L. Bramanti, I. Vielmini, S. Rossi, G. Tsounis, M. Iannelli, R. Cattaneo-Vietti, C. Priori, G. Santangelo, Demographic parameters of two populations of red coral *(Corallium rubrum L. 1758)* in the North Western Mediterranean, Marine Biology 161 (2013) 1015–1026.

[8] G. Galli, L. Bramanti, C. Priori, S. Rossi, G. Santangelo, G. Tsounis, C. Solidoro, Modelling red coral (*Corallium rubrum*) growth in response to temperature and nutrition, Ecological Modelling 337 (2016) 137–148.

[9] J. Gili, R. Coma, Benthic suspension feeders in marine food webs, Trends Ecol. Evol. 13 (1998) 297–337.

[10] J. Garrabou, J. G. Harmelin, A 20-year study on life-history traits of a harvested long-lived temperate coral in the NW Mediterranean: insights into conservation and management needs, Journal of Animal Ecology 71 (2002) 966–978.

[11] F. Giannini, J. Gili, G. Santangelo, Relationships between the spatial distribution of red coral *Corallium rubrum* and coexisting suspension feeders at Medas Islands Marine Protected Areas (Spain), Italian Journal of Zoology 70 (2003) 233–239.

[12] L. L. Price, N. Narchi, Ethnobiology of *Corallium rubrum*: Protection, healing, medicine, and magic, in: Ethnobiology of Corals and Coral Reefs, Springer, 2015, pp. 73–86. doi:10.1007/978-3-319-23763-3_5.

[13] G. Santangelo, M. Abbiati, Red coral: conservation and management of an overexploited Mediterranean species, Aquatic Conservation Marine and Freshwater Ecosystems 11 (2001) 253–259.

[14] M. C. Benedetti, C. Priori, F. Erra, G. Santangelo, Growth patterns in mesophotic octocorals: timing the branching process in the highly-valuable Mediterranean *Corallium rubrum*, Estuarine, Coastal and Shelf Science 171 (2016) 106–110.

[15] C. Priori, V. Mastascusa, F. Erra, M. Angiolillo, S. Canese, G. Santangelo, Demography of deep-dwelling red coral populations: Age and reproductive assessment of a high valuable marine species, Estuarine, Coastal and Shelf Science 118 (2013) 43–49.

[16] L. Bramanti, G. Magagnini, L. D. Maio, G. Santangelo, Recruitment, early survival and growth of the Mediterranean red coral *Corallium rubrum* (L 1758), a 4-year study, Journal of Experimental Marine Biology and Ecology 314 (2005) 69–78.

[17] M. Vighi, Etude sur la reproduction du *Corallium rubrum* (L), Vie et Milieu 23 (1972) 21–32.

[18] I. Gallmetzera, A. Haselmaira, B. Velimirovab, Slow growth and early sexual maturity: Bane and boon for the red coral *Corallium rubrum*, Estuarine, Coastal and Shelf Science 90 (2010) 1–10.

[19] O. Torrents, J. Garrabou, C. Marschal, J.G.Harmelin, Age and size at first reproduction in the commercially exploited red coral *Corallium rubrum* (L.) in the Marseilles area (France, NW Mediterranean), Biological Conservation 121 (2005) 391–397.

[20] G. Santangelo, E. Carletti, E. Maggi, L. Bramanti, Reproduction and population sexual structure of the overexploited Mediterranean red coral *Corallium rubrum*, Marine Ecology Progress Series 248 (2003) 99–108.

[21] E. Zelli, G. Quéré, N. Lago, G. D. Franco, F. Costantini, S. Rossi, L. Bramanti, Settlement dynamics and recruitment responses of Mediterranean gorgonians larvae to different crustose coralline algae species, Journal of Experimental Marine Biology and Ecology 530 (2020) 151427.

[22] O. Torrents, J. Garrabou, Fecundity of red coral *Corallium rubrum*: (L.) populations inhabiting in contrasting environmental conditions in the NW Mediterranean, Marine Biology 158 (2011) 1019–1028.

[23] A. Martínez-Quintana, L. Bramanti, N. Viladrich, S. Rossi, K. Guizien, Quantification of larval traits driving connectivity: the case of *Corallium rubrum* (L. 1758), Marine Biology 162 (2014) 309–318.

[24] K. Guizien, N. Viladrich, Á. Martínez-Quintana, L. Bramanti, Survive or swim: different relationships between migration potential and larval size in three sympatric Mediterranean octocorals, Scientific Reports 10 (2020) 18096.

[25] D. Vielzeuf, J. Garrabou, A. Baronnet, O. Grauby, C. Marschal, Nano to macroscale biomineral architecture of red coral (*Corallium rubrum*), American Mineralogist 93 (2008) 1799–1815.

[26] M. C. Benedetti, L. Bramanti, C. Priori, F. Erra, M. Iannelli, F. Bulleri, G. Santangelo, Polyp longevity in a precious gorgonian coral: hints toward a demographic approach to polyp dynamics, Coral Reefs 39 (2020) 1125–1136.

[27] O. Kahramanoğulları, L. Bramanti, M. C. Benedetti, Stochastic mechanisms of growth and branching in Mediterranean coral colonies, in: Theory and Practice of Natural Computing - 8th International Conference, TPNC 2019, Kingston, ON, Canada, December 9-11, 2019, Proceedings, volume 11934 of *LNCS*, Springer, 2019, pp. 57–69.

[28] M. Grillo, W. Goldberg, D. Allemand, Skeleton and sclerite formation in the precious red coral, *Corallium rubrum*, Marine Biology 117 (1993) 119–128.

[29] D. Allemand, S. Bénazet-Tambutté, Dynamics of calcification in the Mediterranean red coral, *Corallium rubrum* (Linnaeus) (*Cnidaria*, *Octocorallia*), Journal of Experimental Zoology 276 (1996) 270–278.

[30] D. Vielzeuf, J. Garrabou, A. Gagnon, A. Ricolleau, J. Adkins, D. Günther, K. Hametner, J.-L. Devidal, E. Reusser, J. Perrin, N. Floquet, Distribution of sulphur and magnesium in the red coral, Chemical Geology 355 (2013) 13–27.

[31] D. Vielzeuf, A. C. Gagnon, A. Ricolleau, J.-L. Devidal, C. Balme-Heuze, N. Yahiaoui, C. Fonquernie, J. Perrin, J. Garrabou, J.-M. Montel, N. Floquet, Growth kinetics and distribution of trace elements in precious corals, Frontiers in Earth Science 6 (2018) 1–18.

[32] S. Weinberg, Revision of the common Octocorallia of the Mediterranean circalittoral. I. Gorgonacea, Beaufortia 24 (1976) 63–104.

[33] J. Perrin, D. Vielzeuf, A. Ricolleau, H. Dallaporta, S. Valton, N. Floquet, Block-by-block and layer-by-layer growth modes in coral skeletons, American Mineralogist 100 (2015) 681–695.

[34] J. Perrin, C. Rivard, D. Vielzeuf, D. Laporte, C. Fonquernie, A. Ricolleau, M. Cotte, N. Floquet, The coordination of sulfur in synthetic and biogenic Mg calcites: The red coral case, Geochimica et Cosmochimica Acta 197 (2017) 226–244.

[35] C. L. Goff, E. Tambutté, A. A. Venn, N. Techer, D. Allemand, S. Tambutté, In vivo pH measurement at the site of calcification in an octocoral, Scientific Reports 7 (2017) 11210.

[36] M. Valenciennes, Extrait d'une monographie de la famille des gorgonidées de la classe des polypes, Comptes rendus hebdomadaires des séances de l'Académie des sciences, Paris 41 (1855) 7–15.

[37] F. M. Bayer, Contributions to the nomenclature, systematics and morphology of the Octocorallia, Proceedings of the United States National Museum 105 (1955) 207–220.

[38] F. M. Bayer, Recent octocorals, Treatise on Marine Ecology and Paleoecology (ed. H. S. Ladd) Geol. Soc. Amer. Memoir. 67 (1957) 1105–1107.

[39] B. Giordano, L. Bramanti, J. Perrin, O. Kahramanoğulları, D. Vielzeuf, The key role of sclerites in the early life stages of Mediterranean red coral (*Corallium rubrum*), 2022. Submitted.

[40] D. Allemand, The biology and skeletogenesis of the Mediterranean red coral - a review, Precious Corals Octocoral Research 2 (1993) 19–39.

[41] J. C. Lewis, E. V. Wallis, The function of surface sclerites in gorgonians (Coelenterata, Octocorallia), Biological Bulletin Vol. 181 (1991) 275–288.

[42] R. J. Kingsley, Spicule formation in the invertebrates with special reference to the gorgonian *Leptogorgia virgulata*, American Zoologist 24 (1984) 883–891.

[43] D. T. Gillespie, Exact stochastic simulation of coupled chemical reactions, Journal of Physical Chemistry 81 (1977) 2340–2361.

[44] L. Carugati, L. Bramanti, B. Giordano, L. Pittura, R. Cannas, M. C. Follesa, A. Pusceddu, A. Cau, Colonization of plastic debris by the long-lived precious red coral *Corallium rubrum*: New insights on the "plastic benefits" paradox, Marine Pollution Bulletin 165 (2021) 1–7.

[45] D. Allemand, M. C. Grillo, Biocalcification mechanism in gorgonians: 45Ca uptake and deposition by the Mediterranean red coral *Corallium rubrum*, Journal of Experimental zoology 262 (1992) 237–246.

[46] N. Floquet, D. Vielzeuf, Ordered misorientations and preferential directions of growth in mesocrystalline red coral sclerites, Crystal Growth Design 12 (2012) 4805–4820.

[47] N. Floquet, D. Vielzeuf, Mesoscale twinning and crystallographic registers in biominerals, American Mineralogist 96 (2011) 1228–1237.

[48] J. H. Brown, J. F. Gillool, A. P. Allen, V. M. Savage, G. B. Wes, Towards a metabolic theory of ecology, Centennial Special: Notable Papers in ESA History MacArthur Award Series 85 (2004) 1771–1789.

[49] M. Ullah, O. Wolkenhauer (Eds.), Stochastic Approaches for Systems Biology, Springer, 2011.

[50] D. J. Wilkinson (Ed.), Stochastic Modelling for Systems Biology, Third Edition, Chapman and Hall/CRC, 2019.

[51] M. A. Gibson, J. Bruck, Efficient exact stochastic simulation of chemical systems with many species and many channels, Journal of Physical Chemistry 104 (2000) 1876–1889.

[52] Y. Tamura, Mathematical models for understanding phenomena: Vortex-induced vibrations, Japan Architectural Review 3 (2020) 398–422.

[53] K. P. Black, P. J. Morgan, L. S. Hammond, Numerical models show coral reefs can be self-seeding, Marine Ecology Progress Series 71 (1991) 1–11.

[54] P. L. Jokiel, The reef coral two compartment proton flux model: A new approach relating tissue-level physiological processes to gross corallum morphology, Journal of Experimental Marine Biology and Ecology 409 (2011) 1–12.

[55] B. Cafarelli, C. Calculli, D. Cocchi, Bayesian hierarchical nonlinear models for estimating coral growth parameters, Environmetrics 30 (2019) e2559.

[56] S. A. Sandin, Y. Eynaud, G. J. Williams, C. B. Edwards, D. E. McNamara, Modelling the linkage between coral assemblage structure and pattern of environmental forcing, Royal Society Open Science 7 (2020) 1,12.

[57] J. A. Kaandorp, J. E. Kübler, The Algorithmic Beauty of Seaweeds, Sponges and Corals, The Virtual Laboratory, Springer Verlag Berlin Heidelberg, 2001.

[58] H. Meinhardt, P. Prusinkiewicz, D. R. Fowler, The Algorithmic Beauty of Sea Shells, The Virtual Laboratory, Springer Verlag Berlin Heidelberg, 1995.

[59] P. Prusinkiewicz, A. Lindenmayer, The Algorithmic Beauty of Plants, The Virtual Laboratory, Springer Verlag Berlin Heidelberg, 1996.

[60] J. A. Kaandorp, P. M. A. Sloot, Morphological models of radiate accretive growth and the influence of hydrodynamics, Journal of Theoretical Biology 209 (2001) 257–274.

[61] R. Merks, A. Hoekstra, J. Kaandorp, P. Sloot, Models of coral growth: spontaneous branching, compactification and the Laplacian growth assumption, Journal of Theoretical Biology 224 (2003) 153–166.

[62] R. M. H. Merks, A. G. Hoekstra, J. A. Kaandorp, P. M. A. Sloot, Polyp oriented modelling of coral growth, Journal of Theoretical Biology 228 (2004) 559–576.

[63] J. A. Kaandorp, P. M. A. Sloot, R. M. H. Merks, R. P. M. Bak, M. J. A. Vermeij, C. Maier, Morphogenesis of the branching reef coral *madracis mirabilis*, Proceedings of the Royal Society B 288 (2021) 20211260.

[64] C. Laforsch, E. Christoph, C. Glaser, M. Naumann, C. Wild, W. Niggl, A precise and non-destructive method to calculate the surface area in living

scleractinian corals using X-ray computed tomography and 3D modeling, Coral Reefs 27 (2008) 811–820.

[65] N. Chindapol, J. A. Kaandorp, C. Cronemberger, T. Mass, A. Genin, Modelling growth and form of the scleractinian coral *Pocillopora verrucosa* and the influence of hydrodynamics, PLoS Computational Biology 9 (2013) e1002849.

[66] S. J. Hennige, A. I. Larsson, C. Orejas, A. Gori, L. H. D. Clippele, Y. C. Lee, G. Jimeno, K. Georgoulas, N. A. Kamenos, J. M. Roberts, Using the Goldilocks Principle to model coral ecosystem engineering, Proceedings of the Royal Society B 288 (2021) 20211260.

[67] R. Erban, S. J. Chapman, Stochastic Modelling of Reaction–Diffusion Processes, Cambridge University Press, 2020.